Analysis of a Fully Packed Loop Model Arising in a Magnetic Coulomb Phase

L. D. C. Jaubert, M. Haque, and R. Moessner
Max-Planck-Institut für Physik komplexer Systeme, 01187 Dresden, Germany
(Received 31 March 2011; revised manuscript received 5 July 2011; published 18 October 2011)

The Coulomb phase of spin ice, and indeed the I_c phase of water ice, naturally realize a fully packed two-color loop model in 3D. We present a detailed analysis of the statistics of these loops: we find loops spanning the system multiple times hosting a finite fraction of all sites while the average loop length remains finite. We contrast the behavior with an analogous 2D model. We connect this body of results to properties of polymers, percolation and insights from Schramm-Loewner evolution processes. We also study another extended degree of freedom, called worms, which appear as ''Dirac strings'' in spin ice. We discuss implications of these results for the efficiency of numerical cluster algorithms, and address implications for the ordering properties of a broader class of magnetic systems, e.g., with Heisenberg spins, such as $CsNiCrF_6$ or $ZnCr_2O_4$.

DOI: 10.1103/PhysRevLett.107.177202 PACS numbers: 75.10.Hk, 75.10.Kt, 75.60.Ch

In the study of magnetism, we are naturally led to consider local degrees of freedom and their correlations, such as the order of the local spin orientation in a ferromagnet. In other settings, the fundamental degrees of freedom are extended, with polymers presenting perhaps the most familiar instance.

In magnets in two dimensions (2D), linearly extended objects do occur in the form of magnetic domain walls. The study of such ''nonlocal'' degrees of freedom, involving questions such as: ''What is the probability for two bonds to be on the same domain wall?'', is related to problems like the geometry of the hull of a percolating cluster. Some beautiful theories have been developed in this context [1–3]. The same questions in higher dimension do not lend themselves to similarly exact approaches, but fractal extended objects in 3D have been studied in the contexts of polymer physics [4], cosmic strings [5,6], magnetic filaments in manganite materials [7], and laser speckles [8].

Here, we discuss a 3D frustrated magnetic system, spin ice [9], exhibiting two distinct extended degrees of freedom, which we call loops and worms. Spin ice is unusual in that its low-temperature magnetic state is neither ordered (as in a ferromagnet) nor disordered (as in a paramagnet). Rather, this state is a Coulomb phase, where an emergent conservation law leads to algebraic spin correlations [10]. The loops define a two-color fully packed loop model on the diamond lattice (the ''premedial'' lattice of the pyrochlore [11]). Similar loops also emerge in models for pyrochlore compounds with two species of magnetic ions [11–13] or itinerant charges [14,15]. Worms, named after their appearance in Monte Carlo worm algorithms [16,17], only come in one flavor and can pass through themselves and each other. Worms play a conceptually important role in the physics of spin ice as they are connected to ''Dirac strings'' and deconfinement in the Coulomb phase [18–21]. Thus, besides their statistical physics interest, we study loops and worms to elucidate properties of this new magnetic phase.

In this Letter, we numerically evaluate fundamental characteristics such as the probability distribution function (PDF) of loop length ℓ, radius of gyration and the probability for two sites separated by distance r to be on the same loop, $C(r)$. We present analytical arguments to account for the observed regimes and their concomitant power laws, and contrast this behavior to the analogous model in two dimensions, on the checkerboard (Fig. 1), whose premedial lattice is the square lattice. Finally, we mention possible experimental signatures and touch on related models which naturally occur in the study of frustrated magnets and multicolored loop models [11–13].

Loops and worms.—In spin ice, classical Ising spins live on the sites of the pyrochlore, or equivalently, the bonds of

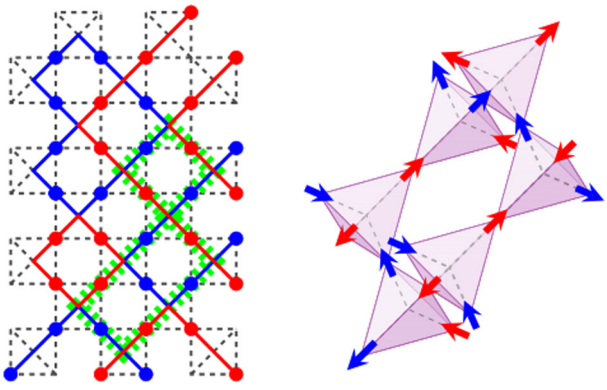

FIG. 1 (color online). Left: Loops of two colors, blue (red) for up (down) spins, and a worm (dashed green, made of alternating up and down spins), on the checkerboard lattice. On the premedial square lattice, every edge is occupied and every site is visited by both loop colors: this is a FPL^2. A worm can cross itself and retrace its path. Right: Spin ice model on the pyrochlore lattice with in (blue) and out (red) spins.

the diamond lattice (Fig. 1). At low temperature, an exponentially large number of degenerate ground state configurations is available, $\exp(NS_p)$, where N is the number of spins and $S_p \approx \frac{1}{2}\log\frac{3}{2}$ is well approximated by Pauling's ice entropy. These states obey the ice rules, stating that two of the spins point towards a given diamond lattice site, the other two pointing outwards. They correspond to the allowed configurations of cubic ice I_c, captured by the six-vertex model on the diamond lattice. The ensemble of these states provides the Coulomb phase exhibiting an emergent gauge field and algebraic correlations [10,11].

By coloring the links occupied by up and down spins differently, we obtain a fully packed two-color loop model (FPL^2 [22], see Fig. 1). In contrast, a worm contains an alternating sequence of adjacent up and down spins. There are different possible constructions for a worm. We adopt an unbiased one in which a worm, having entered a tetrahedron, exits through one of the two opposite spins in that tetrahedron with equal probability. It ends when it meets its initial site.

We consider periodic systems of square or cubic geometry with L unit cells in each direction, so that there are $N_{2D} = 4L^2$ and $N_{3D} = 16L^3$ lattice sites. The smallest possible loop is $\ell_{\min} = 4(6)$ for checkerboard (pyrochlore).

Loop length distributions.—Figure 2 presents the PDF of the loop length obtained using the Monte Carlo worm algorithm [17]. For the checkerboard, the PDF has a single power-law behavior, $P_{2d} \sim \ell^{-\tau}$, with $\tau = 2.14(1)$, in agreement with the exact value $2 + 1/7$ (Refs. [23–25]). The situation is dramatically different for the three-dimensional pyrochlore, where no exact value is available. There are two different power laws: a short loop region where the PDF scales as $\sim L^3\ell^{-2.50(1)}$, and then a crossover at $\ell_1 \sim L^2$ to a large-ℓ region with scaling $\sim\ell^{-0.98(3)}$. The second regime is due to the influence of winding loops, which close only after crossing the periodic boundaries.

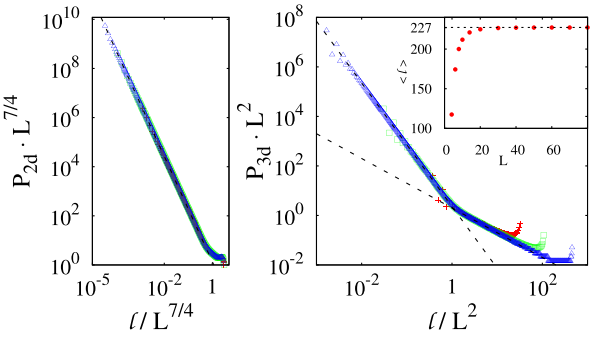

FIG. 2 (color online). Probability distribution of loop lengths ℓ on the checkerboard (left) and pyrochlore (right) lattice, for different system sizes ($L = 100$, 400, 1000 in 2D and $L = 4$, 14, 60 in 3D). Both axes are adequately scaled by $L^{1/\nu}$. Note the absence of one-parameter scaling in 3D at large ℓ. Inset: Average loop length on the pyrochlore lattice, converging with system size to a finite value of 227.3 (dashed line).

We have checked that the PDF of only nonwinding loops has a single power law, $\sim L^3\ell^{-5/2}$. In 2D, the loop distribution is dominated by nonwinding loops at all ℓ. This is reminiscent of Pólya's theorem, that a random walk in 2D is recurrent (always returns to the initial point), while in 3D it is transient (a finite probability never to return) [26]. In both 2D and 3D, $P(\ell)$ increases just before the cutoff at large ℓ.

Winding and nonwinding loop fractions.—In 2D, the average number of winding loops is 1.86(1), whose length scales as $L^{7/4}$. In contrast, in the pyrochlore this number scales as $\ln L$. In both cases the number of nonwinding loops is extensive. The percentage of pyrochlore sites belonging to nonwinding and winding loops are 6.310(5)% and 93.690(5)%, respectively. Thus a finite but small portion of the system is covered by an extensive number of short loops, while most of the lattice sites belong to a few large loops.

Probability to be on the same loop.—In 2D, $C(r) \sim r^{-0.49(1)}$, consistent with [25]. By contrast, in 3D, the leading term in $C(r)$ is a constant (Fig. 3); i.e., sites far from each other have a nonzero probability to be on the same loop—another qualitatively new feature due to winding loops.

Radius of gyration.—This is defined as $R^2 = \frac{1}{\ell}\times\sum_{i=1}^{\ell}|\mathbf{r}_i - \langle\mathbf{r}\rangle|^2$ where $\mathbf{r}_i$ is the position of the ith site of the loop of length ℓ and $\langle\mathbf{r}\rangle = \sum_i \mathbf{r}_i/\ell$. This follows a power law $R \sim \ell^{\nu}$. As discussed in detail later, even though our loops are self-avoiding, we do not find self-avoiding walk exponents (3/4 in 2D and $\approx 3/5$ in 3D), but rather $\nu_{2D} = 0.573(5)$ for nonwinding loops, consistent with 4/7 [23–25] and $\nu_{3D} = 0.500(5)$ as for a random walk.

Brownian motion (BM) analogy.—We account for the above results by adapting the theory of Brownian motion (or random walks or ideal chains) to this setting. The probability for a BM starting at $\mathbf{x_o}$ to visit position $\mathbf{x}$ after ℓ steps, is $p(\mathbf{x_o}, \mathbf{x}; \ell) = (2\pi\ell)^{-3/2}e^{-(\mathbf{x}-\mathbf{x_o})^2/2\ell}$, in the three-dimensional continuum [6,26]. Thus, the probability to come back to the initial point is $p(\mathbf{x_o}; \ell) = (2\pi\ell)^{-3/2}$. Summing over all possible starting positions, one obtains

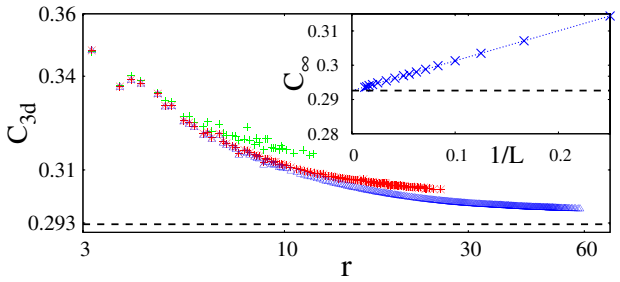

FIG. 3 (color online). Probability for two spins to be on the same loop as a function of the distance between them, on pyrochlore lattices with $L = 4$, 8, 18, asymptoting to $C_\infty = 0.293$ (dashed lines), found by an extrapolation to large system sizes (inset).

for the loop length PDF of nonwinding loops: $P_{3d}^{\mathrm{nw}}(\ell) \approx \frac{1}{\ell}\sum_{\mathbf{x}_o} p(\mathbf{x_o};\ell) \sim L^3\ell^{-5/2}$, where the factor $1/\ell$ compensates the arbitrary starting position along the loop of size ℓ.

To understand the different exponent for large ℓ, we have to consider winding loops. These may be regarded as loops that start at a point in the ''original'' sample but end at an equivalent point in a ''copy'' sample, arising from periodic boundary conditions. The copies cover all space $\mathbb{R}^3$. The probability for the loop reaching the equivalent point in the ith nearest-neighbor copy at distance $r_i = n_i L$, is $P(i;\ell) = (2\pi\ell)^{-3/2} e^{-r_i^2/2\ell}$ in 3D. The number of copies which are ith nearest neighbors scales as $4\pi(r_i/L)^2$ for large i. Thus the total probability for a winding loop starting at $\mathbf{x_o}$ to be of size ℓ is

$$p(\mathbf{x_o};\ell) \approx \sum_{i=0}^{\infty} 4\pi n_i^2 \left(\frac{1}{2\pi\ell}\right)^{3/2} \exp\left[-\frac{n_i^2 L^2}{2\ell}\right] \approx \frac{1}{L^3}.$$

We note that $p(\mathbf{x_o};\ell)$ is independent of ℓ. Summing over all possible initial points, the total probability to have a loop of size ℓ becomes $P_{3d}^{w}(\ell) \approx \frac{1}{\ell}\sum_{\mathbf{x}_o} p(\mathbf{x_o};\ell) \sim \ell^{-1}$, independent of system size L. The crossover between the two behaviors occurs at the length scale $\ell_1 \sim L^2$, i.e., when the radius of gyration of a loop reaches the system size.

The average loop lengths $\langle\ell\rangle$ in both checkerboard and pyrochlore cases are finite. For the checkerboard, the PDF exponent τ being larger than 2 ensures a nondiverging $\langle\ell\rangle_{2\mathrm{D}}$. With the approximation that $P_{2d}(\ell) \propto \ell^{-\tau}$ at all even ℓ starting from $\ell_{\min} = 4$, one estimates

$$\langle\ell\rangle_{2\mathrm{D}} = \left(\sum_{\ell=4,\ell\in 2\mathbb{N}}^{+\infty} \ell.\ell^{-\tau} \Big/ \sum_{\ell=4,\ell\in 2\mathbb{N}}^{+\infty} \ell^{-\tau}\right) \approx 24.9, \quad (1)$$

very close to the numerically obtained average 24.68(3).

For the pyrochlore, the combination of nonwinding ($P_{3d}^{\mathrm{nw}} \sim L^3\ell^{-5/2}$) and winding loops ($P_{3d}^{w} \sim \ell^{-1}$) conspire to produce a remarkably large but finite average loop length: $\langle\ell\rangle_{3\mathrm{D}} = 227.5(5)$. Even though they increase $\langle\ell\rangle_{3\mathrm{D}}$ by an order of magnitude compared to the two-dimensional model, winding loops do not manage to make it divergent.

Considering nonwinding and winding loops separately, the loop length average saturates with L in the former case, $\langle\ell\rangle_{\mathrm{n.w.}} = 14.34(4)$ [Eq. (1) adapted to the pyrochlore gives 15.3], while it diverges as $\langle\ell\rangle_{w} \sim L^3/\ln L$ for winding loops.

Concerning the probability for two sites to be on the same loop, we note that the number of spin pairs belonging to the same loop of length ℓ is $\frac{1}{2}\ell(\ell-1)P(\ell)$, while there is a total of $\frac{1}{2}N(N-1)$ pairs of spins in the system. The probability averaged over all pairs is thus

$$\overline{C(r)} \sim \int_6^{8L^3} \frac{\ell(\ell-1)}{N(N-1)} P_{3d}(\ell)\, d\ell \sim \mathcal{O}(L^0). \quad (2)$$

The nonwinding loop contribution to this integral vanishes at large L, but the winding loop contribution leads to a constant term $C_\infty = C(r\to\infty) = 0.293(2)$ (Fig. 3). Indeed, we note that there will be several winding loops indexed by i in a large system, each of which contains a finite fraction, f_i, of all sites. (We found $f_1 \approx 0.41$, $f_2 \approx 0.30$, $f_3 \approx 0.12\ldots$).

The ''scaling function'' displayed in Fig. 2 shows that two length scales appear in 3D: (i) when the radius of gyration hits the system size, $\ell_1 \sim L^2$, (ii) when the loop explores the full volume, $\ell_2 \sim L^3$. The behavior for $\ell > \ell_1$ obviously is influenced by the nature of the boundary conditions, e.g., the loops winding many times can break up into several loops terminating on the surface [15] when open boundaries are considered.

Worms.—The worms are efficiently evaluated as our Monte Carlo algorithm is in fact based on constructing worms, as flipping all spins in a worm conserves the ice rules. For such a stochastic worm-definition, it is impossible to establish a 1-to-1 mapping between spin and worm configuration. Hence, we compute the probability for a worm starting at a random site $\mathbf{x_o}$ to be of length ℓ; this corresponds to $p(\mathbf{x_o};\ell)$ instead of $P(\ell)$. Again, two regimes appear in 3D, an $\ell^{-3/2}$ behavior (numerical exponent $-1.48(4)$) for $\ell \lesssim \ell_1$, and a ℓ-independent region for larger ℓ, consistent with our BM analogy.

The winding worm regime implies that three-dimensional worms on average visit a finite fraction of the system size ($\approx 15\%$, which is actually less than the average length of a worm, as it can retrace parts of its path). Hence, a worm algorithm only requires a finite (here, of order 10) number of worms to decorrelate the system in 3D, independent of system size L, while the different behavior of winding worms in 2D requires an increasing number of worm updates for decorrelation with L.

Discussion.—Other than the importance of winding loops, a crucial difference between 2D and 3D is the appearance of Brownian motion (BM) exponents for the latter case. This is analogous to polymer solutions at the Θ point [4,27], where the presence of other loops perfectly counteracts the self-avoidance in 3D, but corrections to mean field in 2D make their statistic ($\nu_{2\mathrm{D}} = 4/7$) fall between the one of random walks ($\nu = 1/2$) and self-avoiding walks ($\nu = 3/4$). We next discuss this issue from a different vantage point.

First, note that our two-dimensional loops can be mapped onto a bond percolation problem on the square lattice, with bonds painted in either color with probability $p = 1/2$. While the ice-rules do impose a local constraint, it has been argued that neither short-range nor sufficiently rapidly decaying algebraic long-range correlations (like the r^{-D} correlations in our model) influence the percolation critical exponents [28]. Since loops of the same color cannot cross or branch, each loop is at the same time the external perimeter (''hull'') of a percolation domain,

whose fractal dimension is $D_f = 1/\nu_{2D} = 7/4$ [23]. Also, the number of winding loops should be finite (we find 1.86), as the number of percolating domains is typically of order $\mathcal{O}(1)$ for a square system at criticality.

Now, we can place this in the context of a family of continuous nonbranching growing processes, namely, Schramm-Loewner evolutions $\mathrm{SLE}_{\kappa\in[0:16]}$. Each SLE_κ is described by a 1D Brownian motion with diffusion constant κ, and fractal dimension $D_f = 1 + \kappa/8$, capturing the scaling properties of conformally invariant 2D critical interfaces (see [3] for a review). Hence, we expect our loops with $D_f = 7/4$ to correspond to SLE_6, if any; indeed, percolation hulls can be rigorously identified to SLE_6 [29]. This is also the only SLE_κ process with the locality property [2,3]. Hence the value of $\nu_{2D} = 4/7$ may not only be a correction to mean field, but also a signature of locality. A more direct proof of locality of the loops in the Coulomb phase, without referring to percolation, would be worthwhile investigating.

We note that SLE_6 is also related to BM: it describes the pioneer points, rather than frontier points (with $D_f = 4/3$) or the full BM (for definitions, see footnote [2,30,31]). This identification is *a priori* nontrivial, as all points of nonintersecting walks on a lattice, as our loops, are both pioneer and frontier points. Now in 3D, it appears to us that all points of a BM can be connected to infinity and thus are both pioneer and frontier points, so that these distinctions become moot. This may justify *a posteriori* why the three-dimensional versions of those models—tricolor percolation [32], Θ point [4], and the present work—display the exponent of BM [33]. Further work in this direction, also for other SLE_κ processes, is necessary for a proper understanding of the connection between fractal dimensions in two- and three-dimensional statistical models.

Conceptual and experimental implications.—From many possible analogous models in 2D and 3D, we have managed to identify our loops exponents with those of the pioneer points of a BM. This was not necessarily to be expected *a priori*, as the divergence-free condition of the Coulomb phase, besides creating the loops, imposes much additional structure, such as an emergent gauge field and algebraic spin correlations.

In the context of spin ice, worms play an important conceptual role as they describe the tension-free (emergent) flux loops characteristic of the Coulomb phase. Here we have shown that their statistics resembles that of a Brownian motion in 3D. Since, in a magnetic field $\mathbf{B}$, the worms have been used as an experimental diagnostic of the Coulomb phase [19], a more detailed study as a function of $\mathbf{B}$ would be worthwhile. Indeed, by applying uniaxial pressure, interactions between worms can be tuned [34].

On the two-dimensional front, advances on magnetic lithography make the observation of loops and worms a realistic prospect in artificial spin ice via magnetic force microscopy [35] or x-ray photoemission electron microscopy [36]. Heating-cooling cycles can provide independent sampling, and the average fractal dimension of those loops would be a measure of the influence of the dipolar interactions present in these materials.

To the best of our knowledge, our loops first appeared in Villain's seminal paper in the context of a model of pyrochlore Heisenberg magnets with two species of magnetic ions [12], that could be applied to the $CsNiCrF_6$ compound [11,13]. Villain already noted the possibility of two (recurrent and transient) loop populations, which also show up for cosmic strings [5,6] and laser speckles [8].

In Villain's model, each loop has a distinct color encoding the direction of its Heisenberg spin (which is continuously variable and hence the number of colors is infinite), and spins are correlated only if they belong to the same loop. A finite value of C_∞ thus implies long-range spin order. Here we comment on two noteworthy features. First, the presence of several loops of size $\mathcal{O}(L^3)$ implies coexistence of several spatially intertwined but independent populations of long-range ordered spins, as opposed to the two-color loop model in spin ice materials where the Ising nature of the spin ensures a perfect cancellation of the correlations at long distance, in agreement with algebraically decaying correlations [10]. Second, a short-range interacting classical spin Hamiltonian of the kind envisaged by Villain allows gapless excitations for the Heisenberg spins. Thermal fluctuations out of this set of states could lock these populations into a more conventional collinear ordered structure before destroying the order completely as T increases. As the loops reflect quenched ion disorder in compounds such as $CsNiCrF_6$, the signature of developing (fractal) loop correlations can look highly unconventional when probed with, e.g., neutrons. This is clearly a productive field for more detailed studies, as well as the dynamics of the large interpenetrating clusters.

Indeed, the loops are perhaps most naturally probed as a nonlocal correlation function. For instance, for a system of electrons which can hop only along a loop, the existence of the winding loops shows up in conductivity properties, as we will discuss elsewhere [15].

If one assigns a weight to each loop reflecting the number of flavors, n, it can take (which is not what is done in Villain's model, whose colors are used to distinguish the loops, not to weigh them), it becomes more favorable to have many, short loops as n grows. There is an extended literature on loop models, with some three-dimensional work [37,38], from which it is known that a phase transition results. In our case, an $n = \infty$ state is the "hexagonal protectorate" loop crystal proposed in the context of magnetodistortive phase transitions in the spinel compound $ZnCr_2O_4$ [39]. This has only loops of length 6 and breaks lattice translation symmetry. Further studies of these models, e.g., a quantum version thereof, are ongoing [40].

We thank M. Aizenman, J. Chalker, C. Henley, and V. Pasquier for useful discussions.

[1] B. Duplantier, Phys. Rev. Lett. **81**, 5489 (1998).
[2] G. F. Lawler, O. Schramm, and W. Werner, Acta Math. **187**, 237 (2001); Math. Res. Lett. **8**, 401 (2001).
[3] J. Cardy, Ann. Phys. (Leipzig) **318**, 81 (2005).
[4] P. G. de Gennes, *Scaling Concepts in Polymer Physics* (Cornell Univ. Press, Ithaca, NY, 1979).
[5] A. M. Allega, L. A. Fernández, and A. Tarancón, Phys. Lett. B **227**, 347 (1989).
[6] D. Austin, E. J. Copeland, and R. J. Rivers, Phys. Rev. D **49**, 4089 (1994).
[7] M. Viret *et al.*, Phys. Rev. Lett. **93**, 217402 (2004).
[8] K. O'Holleran, M. R. Dennis, F. Flossmann, and M. J. Padgett, Phys. Rev. Lett. **100**, 053902 (2008).
[9] S. T. Bramwell and M. J. P. Gingras, Science **294**, 1495 (2001).
[10] S. V. Isakov, K. Gregor, R. Moessner, and S. L. Sondhi, Phys. Rev. Lett. **93**, 167204 (2004).
[11] C. L. Henley, Annu. Rev. Condens. Matter Phys. **1**, 179 (2010).
[12] J. Villain, Z. Phys. B **33**, 31 (1979).
[13] S. T. Banks, S. T. Bramwell, T. Fennell, and M. J. Harris (unpublished).
[14] M. Udagawa, H. Ishizuka, and Y. Motome, Phys. Rev. Lett. **104**, 226405 (2010).
[15] L. D. C. Jaubert, M. Haque, S. Pitaecki, and R. Moessner (to be published).
[16] E. L. Pollock and D. M. Ceperley, Phys. Rev. B **36**, 8343 (1987).
[17] G. T. Barkema and M. E. J. Newman, Phys. Rev. E **57**, 1155 (1998).
[18] C. Castelnovo, R. Moessner, and S. L. Sondhi, Nature (London) **451**, 42 (2008).
[19] D. J. P. Morris *et al.*, Science **326**, 411 (2009).
[20] T. Fennell *et al.*, Science **326**, 415 (2009).
[21] A. J. Macdonald, P. C. W. Holdsworth, and R. G. Melko, J. Phys. Condens. Matter **23**, 164208 (2011).
[22] In the ice model, all loops have weight one which, as we shall see, corresponds to a point in the critical regime of FPL^2.
[23] H. Saleur and B. Duplantier, Phys. Rev. Lett. **58**, 2325 (1987).
[24] J. Kondev and C. L. Henley, Phys. Rev. Lett. **74**, 4580 (1995).
[25] J. L. Jacobsen and J. Kondev, Nucl. Phys. **B532**, 635 (1998).
[26] B. D. Hughes, *Random Walks and Random Environments* (Clarendon Press, Oxford, New York, 1995).
[27] B. Duplantier and H. Saleur, Phys. Rev. Lett. **59**, 539 (1987).
[28] A. Weinrib and B. I. Halperin, Phys. Rev. B **27**, 413 (1983).
[29] S. Smirnov, C.R. Acad. Sci. Paris **333**, 239 (2001).
[30] V. Beffara, Ann. Probab. **32**, 2606 (2004).
[31] Let b_τ be a BM point at time τ and $\mathcal{B}_T = \{b_\tau | \tau \in [0;T]\}$ its total trace. b_τ is on the frontier of $\mathcal{B}_T$ if it is not hidden inside its hull, i.e., if it can be connected to infinity without crossing $\mathcal{B}_T$. b_τ is a pioneer point of $\mathcal{B}_T$ if it is on the frontier of $\mathcal{B}_\tau$ [2]. Frontier points have the same fractal dimension as a self-avoiding walk.
[32] R. Mark Bradley, P. N. Strenski, and J.-M. Debierre, Phys. Rev. A **45**, 8513 (1992).
[33] For a study of a negative-weight percolation problem in $D = 2$, 3, 4, see: O. Melchert and A. K. Hartmann, Eur. Phys. J. B **80**, 155 (2011).
[34] L. D. C. Jaubert, J. T. Chalker, P. C. W. Holdsworth, and R. Moessner, Phys. Rev. Lett. **105**, 087201 (2010).
[35] R. F. Wang *et al.*, Nature (London) **439**, 303 (2006).
[36] N. Rougemaille *et al.*, Phys. Rev. Lett. **106**, 057209 (2011).
[37] K. Shtengel and L. P. Chayes, J. Stat. Mech. (2005) P07006, and references therein.
[38] M. Ortuño, A. M. Somoza, and J. T. Chalker, Phys. Rev. Lett. **102**, 070603 (2009); A. Nahum *et al.*, Phys. Rev. Lett. **107**, 110601 (2011).
[39] S. H. Lee *et al.*, Nature (London) **418**, 856 (2002).
[40] N. Shannon (private communication).